This is an open access article published under an ACS AuthorChoice License, which permits copying and redistribution of the article or any adaptations for non-commercial purposes.

JACS
JOURNAL OF THE AMERICAN CHEMICAL SOCIETY

Article

pubs.acs.org/JACS

Ultrafast Charge Transfer in Nickel Phthalocyanine Probed by Femtosecond Raman-Induced Kerr Effect Spectroscopy

Gurusamy Balakrishnan, Alexandra V. Soldatova, Philip J. Reid,* and Thomas G. Spiro*

Department of Chemistry, University of Washington, Seattle, Washington 98195, United States

Supporting Information

ABSTRACT: The recently developed technique of femtosecond stimulated Raman spectroscopy, and its variant, femtosecond Raman-induced Kerr effect spectroscopy (FRIKES), offer access to ultrafast excited-state dynamics via structurally specific vibrational spectra. We have used FRIKES to study the photoexcitation dynamics of nickel(II) phthalocyanine with eight butoxy substituents, $NiPc(OBu)_8$. $NiPc(OBu)_8$ is reported to have a relatively long-lived ligand-to-metal charge-transfer (LMCT) state, an essential characteristic for efficient electron transfer in photocatalysis. Following photoexcitation, vibrational transitions in the FRIKES spectra, assignable to phthalocyanine ring modes, evolve on the femtosecond to picosecond time scales. Correlation of ring core size with the frequency of the ν_{10} (asymmetric C−N stretching) mode confirms the identity of the LMCT state, which has a ∼500 ps lifetime, as well as that of a precursor d-d excited state. An even earlier (∼0.2 ps) transient is observed and tentatively assigned to a higher-lying Jahn−Teller-active LMCT state. This study illustrates the power of FRIKES spectroscopy in elucidating ultrafast molecular dynamics.

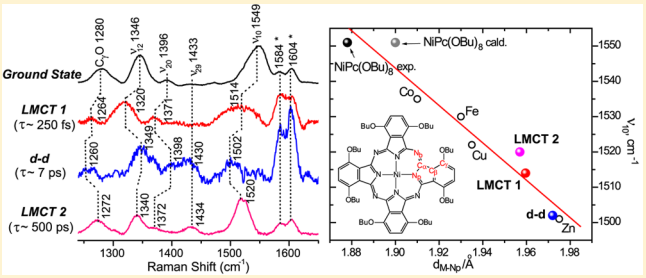

1. INTRODUCTION

Phthalocyanines (Pc's) are of great interest in various applications including molecular electronics, photovoltaics, and photocatalysis, due to their favorable electronic structure and good thermal and chemical stability.[1−5] Because of their intense and tunable light absorption in the red and near-infrared, they are useful as photodynamic and photothermal sensitizers for tumor therapy and other medical applications.[6−8]They also hold promise for dye-sensitized solar cells (DSSCs), given their ability to harvest a greater part of the solar spectrum than current DSSCs employing ruthenium(II) bipyridine-based dyes.[9−13] They could be used as co-sensitizers with dyes having complementary absorption, in tandem solar cells, or via synthetic modification of the macrocycle structure to achieve panchromatic sensitization.[14]

Metallophthalocyanines (MPc's) might also serve as useful photocatalysts, since axial coordination sites of the central metal are available for binding substrate molecules. If photoexcitation leads to ligand-to-metal or metal-to-ligand charge-transfer (LMCT or MLCT) states, then the transiently reduced or oxidized metal could reduce or oxidize bound substrate, provided that recombination is prevented by efficient discharge of the electron or hole on the phthalocyanine ring (for example, by attachment to a semiconductor electrode). The MPc−semiconductor conjugate could then be part of a DSSC, with built-in catalytic capability. The possibility of generating H_2 by photoreduction of water would be particularly appealing. A number of molecular water reduction catalysts are currently under investigation, but they need to work together with a separate absorber for solar applications.[15−20] MPc's offer the possibility of combining the absorber and catalyst in a single molecule.

Realizing the photocatalytic potential of MPc's requires careful tuning of their excited states to ensure that charge separation is sufficiently long to sustain a catalytic reaction. Recently, Gunaratne et al.[21] identified a relatively long-lived excited state in $NiPc(OBu)_8$, the Ni(II) complex of Pc with eight butoxy substituents (Figure 1). They assigned the excited state as a LMCT state from its transient absorption spectral characteristics and the expected energy level ordering from time-dependent density functional theory (TD-DFT) calculations. The reported ∼600 ps lifetime of the LMCT state might permit ring reduction at a p-type semiconductor electrode, making $Ni(I)Pc(OBu)_8$ available for substrate reduction. $NiPc(OBu)_8$ has the added attraction of a substantially red-shifted visible absorption band (Figure 1), increasing its usefulness as a solar absorber.

Structural characterization of the excited states of a potential catalyst is valuable in elucidating the complex mechanism of catalytic transformations. In contrast to transient absorption spectra that are broad and contain little structural information, vibrational spectra typically demonstrate narrow transitions whose frequencies are highly sensitive to structure. Access to ultrafast time-resolved vibrational spectra has recently been facilitated by the development of various coherent Raman spectroscopy (CRS) techniques, such as coherent anti-Stokes Raman spectroscopy (CARS) and femtosecond stimulated

Received: April 9, 2014
Published: May 19, 2014

 © 2014 American Chemical Society dx.doi.org/10.1021/ja503541v | J. Am. Chem. Soc. 2014, 136, 8746−8754

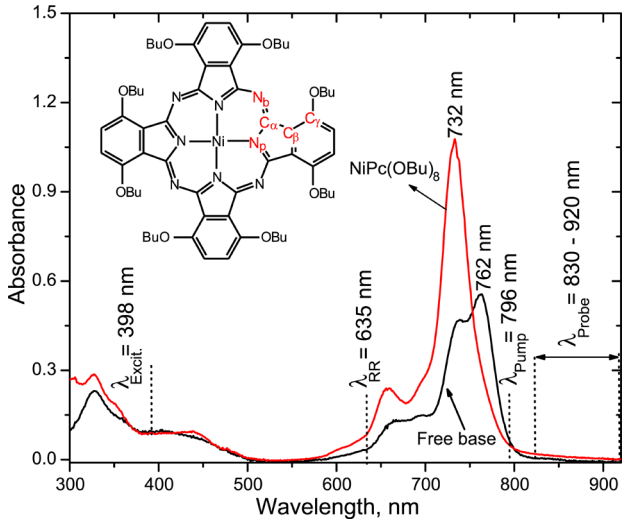

Figure 1. Absorption spectra of octabutoxyphthalocyanine free base (black) and the Ni(II) complex (red) (structure shown in the inset) in toluene. Wavelengths are marked for photoexcitation, resonance Raman excitation, and FRIKES pump and probe lasers.

Raman spectroscopy (FSRS), which are capable of providing Raman spectra with high spectral (<10 cm^{-1}) and temporal resolution (<50 fs).[21−24] Both are nonlinear optical techniques with a directional signal, offering high signal-to-noise ratios with no interference from fluorescence. However, each technique has its own limitations; for example, the intense saturating probe pulses in FSRS require fast reading detectors and a complicated timing sequence, and in CARS, the spectral line shapes are complicated by nonresonant electronic background signal.[22]

Femtosecond Raman-induced Kerr effect spectroscopy (FRIKES) is a polarization-sensitive form of FSRS that measures the depolarized Raman spectrum.[23−26] In FRIKES, the pump pulse induces a birefringence in the medium and exhibits resonances when the difference in frequency between the pump field (ω_p) and Stokes field (ω_S) matches a Raman-active vibrational mode of the medium ($\omega_p - \omega_S = \omega_{vib}$). The pump-induced birefringence causes a polarization change in the Stokes beam, causing a portion of the probe beam to be passed through crossed polarizers as the FRIKES signal. The detected FRIKES signal has been shown to reflect the spontaneous Raman spectrum.[26] Like FSRS, FRIKES provides high signal-to-noise spectra that are insensitive to fluorescence, with vibrational spectral resolution and femtosecond time resolution. In addition, the use of crossed polarizers for detection blocks the strong probe field and avoids saturation of the detector, permitting the use of a conventional charge-coupled device (CCD) with relatively long exposure times. However, FRIKES suffers from a quadratic dependence on concentration,[27] limiting it to molecular systems with strong third-order susceptibility (χ^3) or to relatively concentrated samples, although the present work demonstrates good quality FRIKES spectra at sub-millimolar concentration, due to pre-resonant enhancement. Other strongly absorbing chromophores are likely to be good FRIKES candidates.

Commonly RIKES has been explored in the form of optical heterodyne-detected Raman-induced Kerr effect spectroscopy

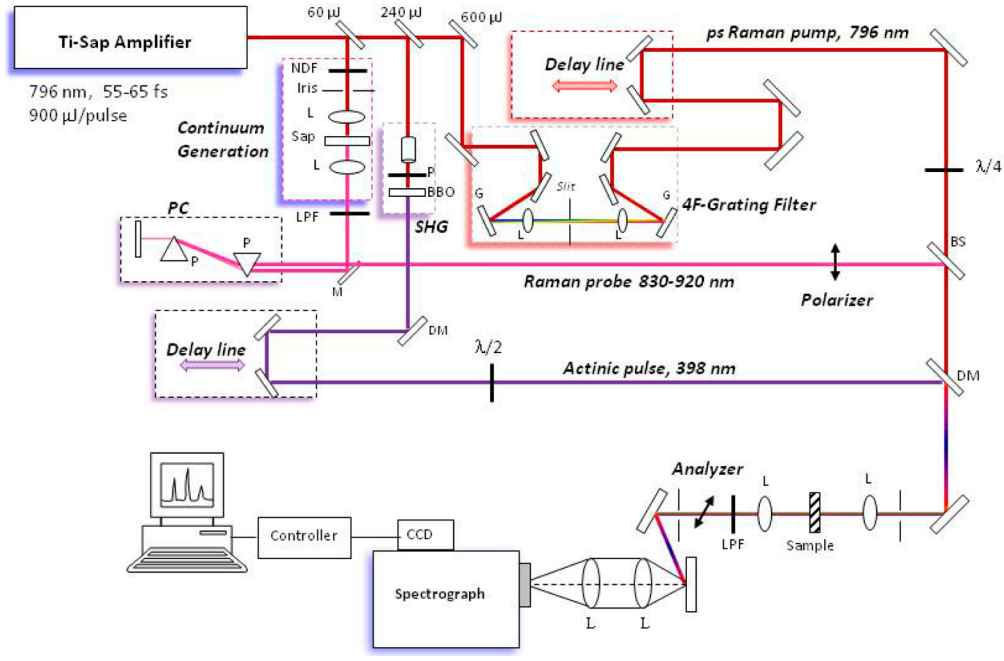

Figure 2. Schematics of the femtosecond Raman-induced Kerr effect spectroscopy (FRIKES) apparatus. The Ti:sapphire amplifier produces a narrow-bandwidth circularly polarized Raman pump (brown) via a 4F-grating-based spatial filter and a $\lambda/4$ plate, a broad-band probe (pink) produced by continuum generation in sapphire, and photoexcitation (violet) via second harmonic generation (SHG) in a BBO crystal. The optical chirp in the continuum is minimized using a prism compressor (PC) made up of a pair of fused silica prisms (P) and a turning mirror. The three pulses are made collinear with a 50:50 beam splitter (BS) and a dichroic mirror (DM), and are all focused at the sample using a single plano-convex lens (L). An 830 nm long-pass filter (LPF) blocks both pump fields as well as the anti-Stokes side of the signal, allowing only the Stokes side of the signal to reach the spectrometer. The crossed polarizer and analyzer configuration permits detection of the pure Raman signal while blocking the background signal from the probe. The signal is recollimated after the sample using a plano-convex lens (L), directed to the collection optics of the Raman spectrometer, and recorded using a CCD detector.

dx.doi.org/10.1021/ja503541v | J. Am. Chem. Soc. 2014, 136, 8746−8754

(OHD-RIKES), using single-wavelength time-domain excitation followed by Fourier transform analysis to obtain depolarized Raman spectra which are limited to the low-frequency region (1−600 cm^{-1}).[28−34] This technique has been applied to study various processes, including the dynamics of pure and mixed solvents,[35−38] electrolyte solutions,[39] ionic liquids,[40−42] polymer solutions,[43] and peptides and globular protein[44] at high concentrations. Studies involving multiplexed RIKES using a broad-band probe are limited.[22,26,45−48] To the best of our knowledge, this is the first study demonstrating the application of FRIKES to the structure and dynamics of photoexcited states in a dilute molecular system.

The excited-state dynamics of $NiPc(OBu)_8$ and of its free-base analogue are characterized by FRIKES in the present work. Our results provide a detailed view of the structural evolution of photoexcited $NiPc(OBu)_8$ and confirm the existence of a relatively long-lived LMCT state, illustrating the power of FRIKES spectroscopy in studying ultrafast molecular dynamics.

2. METHODS

2.1. Materials. Nickel(II) octabutoxyphthalocyanine ($NiPc(OBu)_8$) and free-base octabutoxyphthalocyanine ($H_2Pc(OBu)_8$) were purchased from Sigma-Aldrich and used as received. The solvent toluene (HPLC grade, Fisher Scientific) was used without further purification. Samples were dissolved in toluene, and the concentrations (0.18−0.21 mM) were determined on the basis of the molar extinction coefficients at the absorption maxima (Figure 1) of 732 nm (2.63×10^5 M^{-1} cm^{-1})[21] for $NiPc(OBu)_8$ and 762 nm (1.35×10^5 M^{-1} cm^{-1})[49,50] for $H_2Pc(OBu)_8$. UV−vis absorption spectra were recorded on an Agilent 8453 UV−vis spectrophotometer with a 1 nm slit width using 1 mm path length cells.

2.2. Time-Resolved FRIKES Spectroscopy. Schematics of the experimental setup are shown in Figure 2. A Ti:sapphire oscillator (KM Laboratories) was pumped by the frequency-doubled output of a Nd:YVO_4 laser (Spectra Physics Millennia V), and the oscillator output was used to seed a Ti:sapphire regenerative amplifier (Spectra Physics Spitfire). The seeded regenerative amplifier was pumped by another Nd:YVO_4 laser (Spectra Physics Empower) to produce 55−65 fs pulses (full width at half-maximum) centered at ∼796 nm with an energy of 0.9 mJ/pulse at 1 kHz. About 4−5% of the amplifier output was reflected using a glass flat for continuum generation, and the remainder of the beam was split using a 75/25 beam splitter, with the higher-intensity beam used to generate narrow-bandwidth Raman pump pulses and the lower-intensity beam used to generate actinic pump pulses.

The Raman probe continuum field was generated by focusing a portion of the amplifier output (with reduced beam diameter of 2 mm and 2−3 μJ/pulse) into a sapphire plate (3 mm thick, Meller Optics Inc.), using a plano-convex lens (f = 10 mm). The collimated probe was passed through a long-pass-filter (LPF, 800 nm, Edmund Optics) to block the continuum below 830 nm and a pair of SF10 prisms to compensate for group velocity dispersion. The narrow-bandwidth Raman pump field was obtained through spatial filtering of the high-intensity amplifier beam using a 4F-grating filter procedure.[51,52] Temporal overlap with the probe field was achieved by passing the pump beam through a retroreflector mounted on a manual delay stage. The polarization of the Raman pump was made circular using a zero-order quarter-wave plate (808 nm, ThorLabs). The actinic pump at 398 nm was generated by frequency doubling of the low-intensity amplifier beam using a β-barium borate (BBO) crystal (type-I). Temporal delay of the actinic pump relative to the probe was achieved with a retroreflector mounted on a motorized delay stage (Newport ES300) controlled by Labview software. The polarization of the pump field was set to 54.7° relative to the probe using a zero-order half-wave plate to minimize contributions from rotational dynamics to the optical density evolution. The actinic pump pulse (1.4 μJ/pulse) was made collinear with the Raman pump (2.0 μJ/pulse) and probe using a dichroic mirror (DM), following the collinear combination of Raman pump and probe through a 50:50 beam splitter (BS), and all three pulses were focused at the sample using a single plano-convex lens. Temporal overlap between actinic and Raman pump fields was established using third harmonic generation in a BBO crystal (type II). Measurement of the optical Kerr effect in water at the sample spot was used to establish temporal overlap between actinic pump and probe field and to determine the 180 ± 30 fs time resolution of the apparatus.[53]

After passing through the sample, the signal was collimated and directed to the spectrograph through a long-pass filter (LPF, 800 nm, Edmund Optics) and a polarization analyzer. The LPF blocks both pump and probe fields, as well as the anti-Stokes side of the signal, allowing only the Stokes side of the signal to enter the spectrometer. Two thin-film polarizers (long-pass visible, Thorlabs) with very high extinction ratios of 10^5:1 were used in crossed configuration as polarizer and analyzer and were placed along the probe field before and after the sample to facilitate the detection of the pure Raman signal, while blocking the background probe signal.

The Raman signal was focused into a 0.5-m spectrograph (Acton), equipped with a holographic grating (600 grooves/mm, λ_{blaze} = 800 nm) and a CCD (Pixis 400, Princeton Instruments) operating at −70 °C. The sample solution (0.18−0.21 mM) was circulated through a quartz flow cell (1 mm path length) using a peristaltic pump.

"Probe only" (Raman pump off) and "pump + probe" (Raman pump on) signals were collected, and their ratio [(pump on)/(pump off)] provided the FRIKES (or Raman gain) spectrum. Both signals were averaged over 30 × 1 s accumulations. Time-resolved FRIKES spectra following photoexcitation by the actinic pulse were measured by varying the delay between the actinic pump and Raman probe at 67 time points spanning −4 to 850 ps, spaced equally on a log scale. During the time-resolved experiment, the ground-state FRIKES spectrum was measured periodically (eight times) to check the sample integrity and the laser stability. The overall signal fluctuation was estimated to be ±2% from the FRIKES spectra measured over the course of 3 h. The ground-state spectral intensity declined about 3.5% during the entire measurement (Figure S1), showing minimal sample decomposition. The measured spectra were calibrated using the Raman spectrum of cyclohexane and toluene.

Light Field software (Princeton Instruments) was used to control the CCD and collect the Raman spectra, and MS Excel 2007, Grams/AI 7.00 (Galactic Industries Corp.), and Microcal Origin 6.0 were used to process, analyze, and plot the data.

2.3. Resonance Raman Spectroscopy. Resonance Raman (RR) spectra were obtained using 635 nm (5 mW, Aixiz laser diode) excitation light focused on the spinning sample NMR tube (5 mm glass). The scattered light was collected at 135° with a pair of fused quartz lenses, f-matched to a 0.5 m spectrograph. The spectrograph and detector are the same as described above for FRIKES. Spectra were averaged for 10 min. The same concentrations of the phthalocyanine solutions were used as in FRIKES experiments (0.18−0.21 mM).

3. RESULTS

$NiPc(OBu)_8$ was chosen to test the applicability of the FRIKES technique to a dynamic molecular system of technological importance. Its free-base analogue, $H_2Pc(OBu)_8$, was included in the FRIKES study for comparison. The $NiPc(OBu)_8$ ground- and excited-state electronic structures and its excited-state dynamics have been studied thoroughly by ultrafast transient absorption coupled with DFT/TD-DFT methods.[21] The ground-state absorption spectra of $NiPc(OBu)_8$ and $H_2Pc(OBu)_8$ in toluene, as well as the laser wavelengths used to obtain FRIKES and RR spectra and for photoexcitation, are shown in Figure 1. Consistent with previous reports,[49,50] the $H_2Pc(OBu)_8$ spectrum shows characteristic splitting of the Q(0,0) band into Q_x and Q_y components, due to lowered symmetry of the ring; vibrational peaks are seen to the blue of

dx.doi.org/10.1021/ja503541v | J. Am. Chem. Soc. 2014, 136, 8746−8754

the main Q-band. Upon Ni(II) insertion into the macrocycle, the Q_x and Q_y bands collapse and blue-shift, resulting in a single Q-band at 733 nm. Excitation at 635 nm produced a strong, broad fluorescence spectrum for $H_2Pc(OBu)_8$, centered at 780 nm (Figure S1),[54] which was substantially quenched in $NiPc(OBu)_8$. The fluorescence signal from $NiPc(OBu)_8$ is attributable to a residual free-base impurity, estimated to be about 5%.

3.1. Ground-State RR and FRIKES Spectroscopy of $NiPc(OBu)_8$. Raman gain spectra are best excited in the pre-resonant region, where the electronic resonance provides significant enhancement but sample light absorption remains modest.[55−57] The FRIKES pump and probe wavelengths satisfy this criterion, being slightly below the red edge of the Q(0,0) bands. When spontaneous RR spectroscopy was attempted in this region, the Raman signal was overwhelmed by the broad fluorescence due to the free-base impurity. However, a RR spectrum of $NiPc(OBu)_8$ was obtained by exciting on the blue side of the Q envelope at 635 nm (Figure 1). The RR spectrum (Figure 3, bottom) demonstrates several transitions assignable

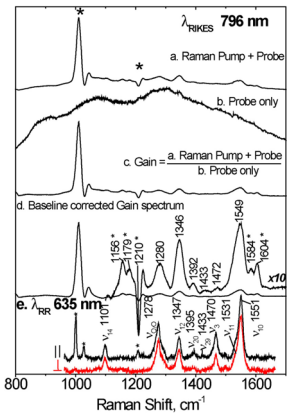

Figure 3. FRIKES spectra of $NiPc(OBu)_8$ in toluene with a 796 nm pump, and the polarized RR spectrum excited at 635 nm. The normal-mode labeling is based on assignments for copper phthalocyanine.[80]

to vibrational modes of the macrocycle. All of them except one (1470 cm^{-1}, ρ = 0.52) were found to be depolarized and correspond to non-totally symmetric modes. In porphyrins, Q-band-resonant enhancement of non-totally symmetric modes is due to Hertzberg−Teller coupling between the weak Q and the stronger, higher-lying B electronic transitions.[58−61] Phthalocyanines, however, have strong Q transitions, and Franck−Condon scattering is expected to dominate, as has been observed.[62−66] Instead, enhancement of non-totally symmetric modes is attributable to a Jahn−Teller (J-T) effect in the doubly degenerate π-π^* excited state.[67−70]

Vibrational spectra of free-base and a variety of metal-bound phthalocyanines have been extensively studied experimentally via Raman, RR, and infrared spectroscopy and analyzed through high-level DFT calculations.[62−66,71−78] The $NiPc(OBu)_8$ RR spectrum between 1100 and 1600 cm^{-1} (Figure 3, bottom) is dominated by phthalocyanine ring vibrations. The bands between 1390 and 1480 cm^{-1} are due to isoindole ring stretching, while the most intense band, at 1551 cm^{-1}, is assigned to $C_\alpha-N_b-C_\alpha$ bridge bond stretching. A localized 1101 cm^{-1} band arises from the breathing vibration of the pyrrole unit. The 1551 cm^{-1} $C_\alpha-N_b-C_\alpha$ bridge stretch is of considerable significance, as it has been shown to be sensitive to the central metal in phthalocyanine, correlating with the size of the macrocycle core.[79] In the present study, this transition undergoes a substantial frequency shift during the evolution of the time-resolved FRIKES spectrum and serves as a spectroscopic marker of the excited-state decay pathway (*vide infra*).

Table 1 lists suggested assignments of the 635-nm-excited RR bands of $NiPc(OBu)_8$, based on assignments for copper

Table 1. Raman Frequencies, Labeling, and Vibration Mode Descriptions of H_2- and $NiPc(OBu)_8$

frequency (cm^{-1})				
$H_2Pc(OBu)_8$	$NiPc(OBu)_8$	description[a]	symmetry	mode[b]
1524	1551	$\nu C_\alpha N_b$	B_{1g}	ν_{10}
	1531	$\nu C_\alpha C_\beta/\nu C_\alpha N_b/\nu C_\beta C_\beta$	A_{1g}	ν_{11}
	1470	$\nu C_\alpha N_b/\delta N_p C_\alpha C_\beta/\delta CH$	B_{2g}	ν_3
1425	1433	$\nu C_\beta C_\beta/\delta CH$	A_{1g}	ν_{29}
	1395	$\nu C_\alpha N_p/\delta C_\alpha N_b C_\alpha/\nu C_\delta C_\delta$	A_{1g}	ν_{20}
1337	1347	$\nu C_\beta C_\beta/\delta C_\alpha N_p C_\alpha/\nu C_\beta C_\gamma/\nu C_\gamma C_\delta$	A_{2g}	ν_{12}
1281	1278	$\nu C_\gamma O$		
	1101	$\delta C_\alpha N_p C_\alpha/\nu NiN_p$	A_{1g}	ν_{14}

[a]See Figure 1 for atom labeling. [b]Mode labeling is adapted from ref 80.

phthalocyanine by Smith and co-workers,[80] and extended by Basova et al.[81] through ^{15}N labeling, single-crystal polarized Raman spectra, and DFT calculations. The mode labeling is by analogy with the scheme widely used for porphyrins, as suggested by Smith and co-workers.[80] (The "g" and "u" symmetry labels appropriate for D_{4h} molecular symmetry are retained, even though the $NiPc(OBu)_8$ macrocycle is distinctly saddled due to steric crowding of the butoxy substituents.[21,82]) Except for the 1470 cm^{-1} band, assigned to the totally symmetric mode, ν_3, the measured depolarization ratios are all close to 0.75, indicating B_{1g} or B_{2g} modes. One band, 1278 cm^{-1}, does not have a correspondence in the CuPc spectrum and is suggested to arise from a mode involving the ring-O stretch of the butoxy substituents; the ring-O stretch of phenoxy compounds is commonly found in this region.[83−85]

The FRIKES experiment with 796 nm excitation provides a background-free Raman spectrum of $NiPc(OBu)_8$ (Figure 3). The gain spectrum is obtained by dividing the "pump + probe" signal by the "probe only" signal followed by baseline correction using a cubic spline function. The high signal-to-noise ratio provides a well-resolved solute spectrum, even in the presence of the very strong solvent Raman bands (marked with asterisks). The solvent bands are both positive and negative because of a complex FRIKES dependence on the Raman pump polarizer angles. The FRIKES intensity was found to vary from positive to negative as the pump pulse polarization was tuned from circular to slightly elliptical, in a complex manner dependent on band position and polarization, as well as on the electronic absorption spectrum. This pump polarization dependence of FRIKES intensity will be reported elsewhere. We chose the Raman pump polarization that maximized the solute signals. The solvent signals are altered by the presence of the solute and therefore cannot be subtracted out straightforwardly.

The $NiPc(OBu)_8$ FRIKES bands are found at the same positions as the 635 nm excited RR bands (Figure 3), but with different relative intensities, reflecting the different resonance

dx.doi.org/10.1021/ja503541v | J. Am. Chem. Soc. 2014, 136, 8746−8754

conditions. Also, the FRIKES bands are broader (fwhm = 28 cm^{-1}), compared to RR (fwhm = 14 cm^{-1}), due to the broader line width (~10 cm^{-1}) of the picosecond Raman pump pulse in FRIKES compared to the narrower line width (<0.1 cm^{-1}) of the continuous-wave laser in RR excitation.

Spontaneous RR spectra for $H_2Pc(OBu)_8$ could not be obtained, even with 635 nm excitation, due to the strong fluorescence background. Its FRIKES spectrum (Figure 4, left, probe spectrum) is similar to that of $NiPc(OBu)_8$, with bands shifted to lower frequency, reflecting a larger macrocycle core in free-base phthalocyanine (Table 1). However, fewer Raman-active bands in the 1390−1480 cm^{-1} region are enhanced.

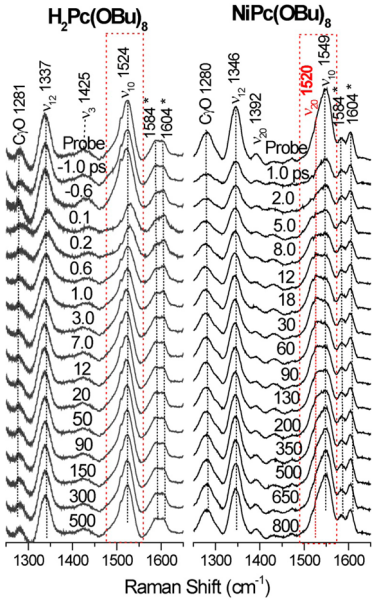

Figure 4. Time-resolved FRIKES spectra of $H_2Pc(OBu)_8$ (left) and $NiPc(OBu)_8$ (right) in toluene at the indicated delay times. The ground-state (probe) spectrum is included at the top for comparison. Solvent bands are indicated with asterisks.

3.2. Photoinduced FRIKES Dynamics of $H_2Pc(OBu)_8$. Photoinduced FRIKES spectra of $H_2Pc(OBu)_8$ were examined as a control for the more complex dynamics of $NiPc(OBu)_8$. Introduction of the 398 nm actinic pump produced an instantaneous bleach, followed by recovery of the ground-state spectrum on the picosecond time scale (Figure 4). The intensity recovery time course for the two strong FRIKES bands at 1524 and 1337 cm^{-1} (Figure 5) yields a time constant of 167 ± 10 ps, assigned to the decay of the photoexcited state. Recovery of the ground state occurs mainly through non-radiative decay from the S_1 state. This decay time is comparable to the 130 ps nonradiative decay time reported for free-base phthalocyanine tetrasulfonate in DMSO.[86] Similar nonradiative decay time constants, ranging from 54 to 277 ps, have been reported for substituted corroles.[87] The intensity recovery time profile also contains a small baseline, possibly due to long-lived fluorescence ($\tau_{fluorescence}$ = 4.2 ns in ethanol for $H_2Pc(OBu)_8$)[88] and/or formation of the triplet $^3(\pi\text{-}\pi^*)$ state that is expected to occur with small quantum yield.[49]

As they recover, these bands also shift to slightly higher frequencies (~2 cm^{-1}), with a complex time dependence (Figure S3), which we attribute to vibrational cooling in the ground state. Importantly, however, no new photoinduced transient spectrum is detectable, in contrast to $NiPc(OBu)_8$ (see below).

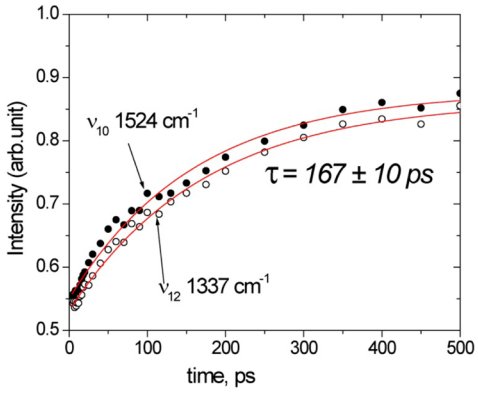

Figure 5. Bleaching and recovery kinetics of $H_2Pc(OBu)_8$ in toluene following photoexcitation at 398 nm, obtained from the intensities (heights) of the ground-state Raman bands at 1524 and 1337 cm^{-1}.

3.3. Photoinduced FRIKES Dynamics of $NiPc(OBu)_8$. Similar to $H_2Pc(OBu)_8$, the time-resolved FRIKES spectra of $NiPc(OBu)_8$ also show bleaching and recovery of the ground-state bands following 398 nm photoexcitation. Unlike $H_2Pc(OBu)_8$, the $NiPc(OBu)_8$ bands undergo significant broadening and frequency shifts to lower wavenumber (see Figure 4, highlighted region with red box), which can be resolved into distinct intermediate spectra by subtracting the ground-state spectra from the transient spectra, using the intensity of the strongest ground-state band (ν_{10}) as a normalization factor. In the ultrafast region (0−1 ps), the three main bands (ν_{10}, ν_{12}, and $\nu_{ring\text{-}O}$) have shifted to much lower frequencies (Figure 6) and are substantially broader than in the ground state. These bands arise within the instrument response time and decay on the femtosecond time scale, with a time constant of ~200 fs (Figure 7a).

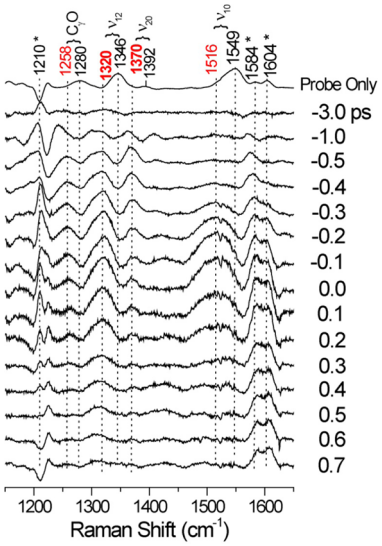

Figure 6. Difference FRIKES spectra (photoexcited − probe only) of $NiPc(OBu)_8$ in toluene at the indicated early delay times. The ground-state (probe only) spectrum is included at the top for comparison. The bands indicated with red labels exclusively correspond to the transient-state bands.

dx.doi.org/10.1021/ja503541v | J. Am. Chem. Soc. 2014, 136, 8746−8754

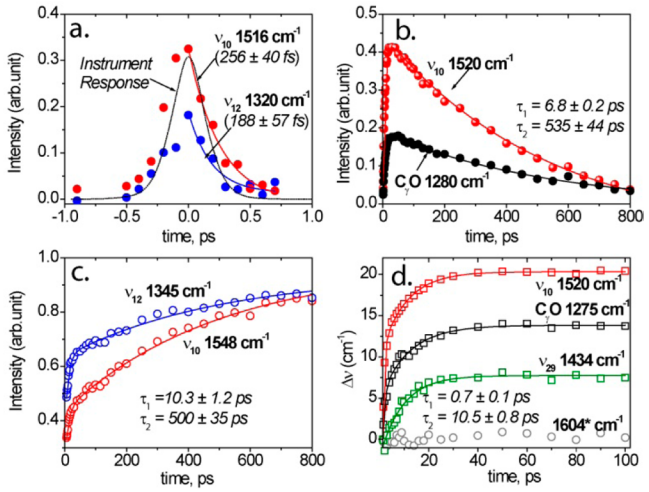

Figure 7. (a) Ultrafast evolution of the excited-state modes of NiPc(OBu)$_8$ in toluene. The continuous line corresponds to a single-exponential decay fit. The instrument response function measured using the optical Kerr effect of water is shown as a black line. Time plots are shown for the intensities (b) and frequencies (d) of the indicated modes of the NiPc(OBu)$_8$ species 3. (c) Bleaching and recovery kinetics of NiPc(OBu)$_8$ in toluene following photoexcitation at 398 nm, obtained from the intensities (heights) of the indicated ground-state bands.

On the picosecond time scale, the ν_{10} and $\nu_{\text{ring-O}}$ bands shift to even lower frequencies (Figure 8, inset) and then recover to

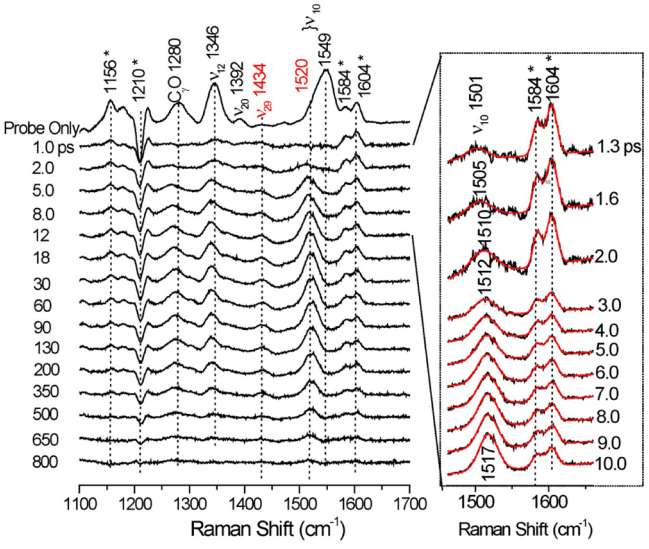

Figure 8. Difference FRIKES spectra (photoexcited − probe only) of NiPc(OBu)$_8$ in toluene at the indicated delay times. The ground-state (probe only) spectrum is included at the top for comparison. The bands indicated with red labels exclusively correspond to the transient-state bands. The expanded spectra between 1.3 and 10 ps are shown on the right for clarity. The ν_{10} peak positions were obtained by spectral deconvolution (red traces).

an intermediate position before returning to the ground-state values (Figure 8); the intensity rise and decay times of these intermediate frequencies are 6.8 and 535 ps, respectively (Figure 7b). In addition, the time courses of the frequency shifts, shown in Figure 7d, follow the ∼10 ps lifetime of the intensity rise but have an extra fast component of ∼0.7 ps.

In summary, the time-resolved FRIKES spectra identify three different species, with distinct frequencies for the Pc ring vibrations. The first species is generated instantaneously, with its core-size marker frequency ν_{10} well below that of the ground state. Species 1 decays with a ∼200 fs lifetime to generate a second species with even lower ν_{10} frequency, which then evolves into a third species on the ∼10 ps time scale, with an intermediate ν_{10} frequency. The third species then decays to the ground state, with a time constant of ∼535 ps. The band frequencies for these species are listed in Table 2, while Figure 9 compares spectra at time points 0.1, 1.3, and 20 ps, where these species predominate.

Table 2. Comparison of FRIKES Frequencies (cm^{-1}) of NiPc(OBu)$_8$ in the Ground State and in Different Excited States along the Excited-State Deactivation Pathway

mode	ground state	species 1	species 2	species 3
ν_{10}	1549	1514	1502	1520
ν_{29}	1433		1430	1434
ν_{20}	1392	1371	1398	1372
ν_{12}	1346	1320	1349	1340
νC$_\gamma$O	1280	1264	1260	1272

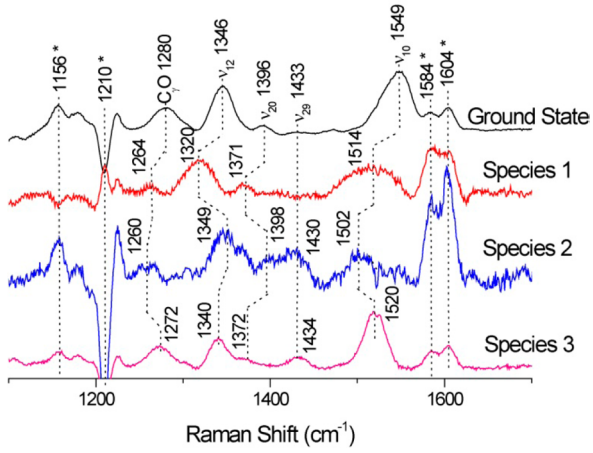

Figure 9. FRIKES spectra of NiPc(OBu)$_8$ in toluene in its ground states and at the time points (0.1, 0.3, and 20 ps) where the indicated transient species are expected to predominate.

The time course of NiPc(OBu)$_8$ ground-state recovery (Figure 7c) has two phases of comparable amplitude, with time constants of 10.3 and 500 ps that are similar to the decay time constants for the second and third intermediate species. This behavior suggests branching for the second intermediate between decay to the ground state and to the third intermediate, with about 50% population decay to each.

4. DISCUSSION

Previous transient absorption spectroscopic study of NiPc(OBu)$_8$ identified two intermediates following photoexcitation within the Q absorption band.[21] With the aid of TD-DFT computations, these intermediates were assigned to a d-d excited state [^{3}(d_{z^2}-$d_{x^2-y^2}$)] and to a LMCT [^{3}(π-$d_{x^2-y^2}$)] state, having ∼18 and 640 ps lifetimes, respectively. The assignments were supported by comparison of spectral changes with reference spectra of species with analogous electronic structure. However, absorption spectra are broad and lack structural specificity. Vibrational spectra, which reflect changes in

dx.doi.org/10.1021/ja503541v | J. Am. Chem. Soc. 2014, 136, 8746−8754

geometry and bond strength, are more discriminating with respect to structure. The FRIKES technique offers access to excited-state vibrational spectra with ultrafast time resolution. We find that the time-resolved FRIKES spectra of photoexcited $NiPc(OBu)_8$ support the interpretation of Gunaratne et al.[21]

The characteristic band frequencies and polarizations of the ground-state $NiPc(OBu)_8$ FRIKES spectrum afford reliable assignments to modes of the Pc macrocycle, involving stretching of the ring C−N and C−C bonds.[62−66,71−78] These bonds are responsive to changes in macrocycle geometry and in the occupancy of the macrocycle π orbitals. In particular, expansion of the macrocycle core, as a result of increasing the central metal radius, produces characteristic downshifts in the macrocycle ring modes. Also important are changes in the π electron density of the macrocycle (which can also affect core size). Tackley et al.[79] have examined RR spectra for a series of structurally characterized MPc's, and a plot of their data for the ν_{10} band is presented in Figure 10. The ν_{10} mode mainly

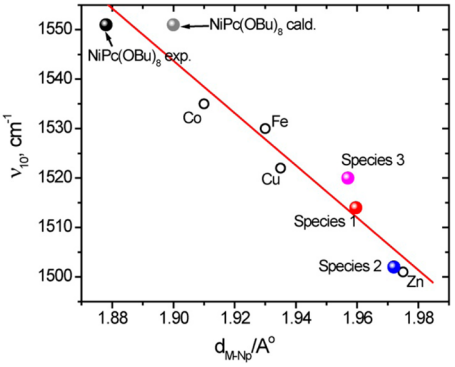

Figure 10. Correlation of ν_{10} frequency with M−N_p (Å) distance in various metallophthalocyanines (from ref 79) and in photoexcited transients of $NiPc(OBu)_8$ studied here (see text for details). Species 1 Ni−N_p distance value is an estimate derived from FRIKES.

involves stretching of the Pc azo-bridge bonds. Its frequency shows the expected negative correlation with core size, similar to that documented for metalloporphyrins,[89] for which ν_{10} involves the methine bridges. As seen in Figure 10, the point for $NiPc(OBu)_8$ falls satisfactorily on the correlation line (the value for the Ni−N_p bond length is from the crystal structure[21]), in the top left corner, consistent with the small ionic radius of Ni, which requires contraction of the macrocycle cavity for effective bond formation. The core-size dependence of ν_{10} provides a key to structural interpretation of the FRIKES spectra.

We now consider the structures of the three photo-intermediates identified in the FRIKES spectra. The species 3 decay time, 500 ps, is similar to that reported by Gunaratne et al.[21] for their final absorption intermediate (640 ps), which they assigned to a LMCT state (1^3A_2), described as a macrocycle−π HOMO to metal−$d_{x^2-y^2}$ transition. The metal-derived $d_{x^2-y^2}$ orbital is heavily mixed with the macrocycle's N_p lone pairs in antibonding fashion; hence, an expanded Pc core is expected. Indeed, the DFT-computed Ni−N_p bond distance is 1.957 Å for this state, 0.057 Å longer than that computed for the ground state.[21,82] The ν_{10} frequency for species 3, which is 30 cm^{-1} lower than the ground-state frequency, falls on the correlation plot at the DFT-computed Ni−N_p distance (Figure 10), close to the Cu-phthalocyanine point, where $d_{x^2-y^2}$ is populated, thus confirming the LMCT assignment for species 3.

From the transient absorption study[21] it was concluded that the LMCT state evolves from another intermediate, which was assigned to a d-d state (1^3B_2), arising from the metal d_{z^2} to $d_{x^2-y^2}$ one-electron transition. The associated difference absorption feature appeared and decayed with time constants of 2 and 21 ps, respectively. Also its peak wavelength blue-shifted during this time, suggesting vibrational cooling of the initially formed vibrationally hot state. We associate this intermediate with FRIKES species 2, which evolves to species 3 in ∼7 ps. The stronger FRIKES intensity of the species 3 bands is mainly responsible for the apparent upshift in the species 2 frequencies as time evolves (Figure 9), but vibrational cooling of species 3 may also contribute. The even lower species 2 frequencies indicate an even more expanded Pc core in the d-d than in the LMCT state. Indeed, the computed 1^3B_2 Ni−N_p distance is 1.972 Å, 0.015 Å longer than for the ^{3}LMCT 1^3A_2 state, presumably because, although the antibonding $d_{x^2-y^2}$ orbital is occupied in both the LMCT and d-d states, the Pc ring is neutral in the latter but is positively charged in the former, which therefore undergoes a slight contraction. The species 2 frequencies fall on the correlation plot at the computed 1^3B_2 Ni−N_p distance, thus confirming a d-d assignment.

The prompt FRIKES intermediate with ∼0.2 ps decay, species 1, was not detected in the transient absorption measurements of Gunaratne et al.,[21] although their time resolution was similar to ours. The main difference in the two studies is that Gunaratne et al.[21] used 660 or 730 nm excitation, in the Q absorption band, while our actinic laser was at 398 nm, in the B absorption band (Figure 1). Consequently, species 1 is attributed to a state arising from S_2 excitation. However, it is unlikely to represent S_2 itself, because a similar species is not detected in the FRIKES spectra of the free base, $H_2Pc(OBu)_8$, which was also excited in its B band. A likely candidate is a higher-lying LMCT state, 2^3E, involving excitation from deeper Pc π orbitals to the Ni. This state was computed[21] to lie only 0.24 eV above the S_1 state, vertically, and relaxation might lower it below S_1, providing an efficient deactivation route. The Pc orbitals are of e_g symmetry, and their excitation would produce a J-T distortion,[67−70] facilitated by the B_g modes that are enhanced in the FRIKES spectrum. The breadth of the species 1 bands, and their depressed frequencies, are consistent with a dynamic J-T effect, as the degenerate π orbitals interconvert. We note as well the large (25 cm^{-1}) frequency drop for the modes ν_{12} and ν_{20} in species 1 relative to the ground state and to species 2, the d-d state. These modes mainly involve the isoindole rings[80] and should be little affected by the altered metal orbital occupation in the d-d state. They are, however, sensitive to the removal of an electron from the Pc π orbitals, and the frequency decrease is amplified by the J-T effect. The LMCT state assigned to species 3 is non-degenerate and not J-T active; its ν_{12} and ν_{20} frequency lowerings from the ground state are smaller (6 and 20 cm^{-1}) than those of species 1.

A diagram of the inferred excited-state dynamics of $NiPc(OBu)_8$ is given in Figure 11. Photoexcitation to the S_2 state is immediately followed by conversion to a J-T-active LMCT state, which relaxes in 0.3 ps to an excited d-d state. The d-d state lives for ∼7 ps, its decay branching between return to the ground state and conversion to the LMCT state, which subsequently decays with a 500 ps lifetime. We note that the transient absorption experiment[21] also could not rule out the possibility of a direct repopulation of the ground state from the

dx.doi.org/10.1021/ja503541v | J. Am. Chem. Soc. 2014, 136, 8746−8754

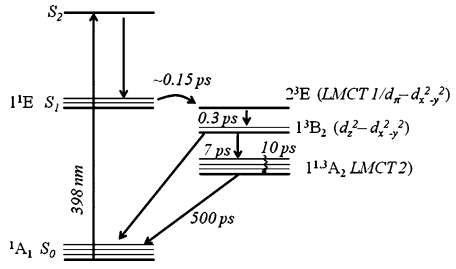

Figure 11. Schematic energy level diagram for $NiPc(OBu)_8$ in toluene following photoexcition at 398 nm by the actinic pump pulse. States are labeled as given in ref 21.

d-d state (with 10 ps lifetime), which could happen in parallel to its decay to the LMCT state.

5. CONCLUSIONS

FRIKES spectroscopy is a powerful technique for probing ultrafast molecular dynamics with structural specificity. As with FSRS, the sensitivity conferred by stimulated Raman gain permits the acquisition of Raman spectra of low-abundance species in short acquisition times. FRIKES has the added advantage of eliminating the strong probe pulse background via tuning of the polarization.

This technique has enabled us to track the vibrational spectrum of a phthalocyanine free base and its Ni(II) complex in the femtosecond to nanosecond time regime following photoexcitation, permitting detailed characterization of the excited-state dynamics. We confirm the proposal of Gunaratne et al.,[21] that relaxation of photoexcited $NiPc(OBu)_8$ proceeds via an excited d-d state to a LMCT state, in which charge separation persists for ~0.5 ns. Remarkable support for the identification of these excited states is provided by the excellent agreement of the phthalocyanine core size, as deduced from the vibrational frequencies, with the DFT/TD-DFT-computed structures. In addition, we found a new ultrafast species, suggested to be a higher-lying, Jahn−Teller-active LMCT state, arising from photoexcitation to the S_2 level. These results emphasize the importance of charge transfer to and from the metal ion in metallophthalocyanines, and their potential for energy storage and energy dissipation.

The structural detail afforded by the FRIKES technique, along with its high sensitivity and ultrafast time resolution, offers great promise for the elucidation of complex molecular systems in chemistry and biology.

■ ASSOCIATED CONTENT

Supporting Information

Repeated measurements of ground-state FRIKES spectra of $NiPc(OBu)_8$ during the time-resolved experiments for the sample integrity, emission spectra of $H_2Pc(OBu)_8$ and $NiPc(OBu)_8$ samples, and time dependence of the ground-state frequencies of $H_2Pc(OBu)_8$. This material is available free of charge via the Internet at http://pubs.acs.org.

■ AUTHOR INFORMATION

Corresponding Authors

pjreid@uw.edu
spiro@chem.washington.edu

Notes

The authors declare no competing financial interest.

■ ACKNOWLEDGMENTS

This work was supported by NIH grant GM 25158 and NSF grant CHE 1068250 (to T.G.S.) and NSF grant DMR 100589 (to P.J.R.). We thank Prof. Richard Mathies and Dr. David Hoffman for helpful advice on the construction of the FRIKES apparatus.

■ REFERENCES

(1) Claessens, C. G.; Hahn, U.; Torres, T. *Chem. Rec.* **2008**, *8*, 75−97.
(2) Elemans, J.; Van Hameren, R.; Nolte, R. J. M.; Rowan, A. E. *Adv. Mater.* **2006**, *18*, 1251−1266.
(3) de la Torre, G.; Claessens, C. G.; Torres, T. *Chem. Commun.* **2007**, 2000−2015.
(4) Lin, C. F.; Zhang, M.; Liu, S. W.; Chiu, T. L.; Lee, J. H. *Int. J. Mol. Sci.* **2011**, *12*, 476−505.
(5) Bottari, G.; de la Torre, G.; Guldi, D. M.; Torres, T. *Chem. Rev.* **2010**, *110*, 6768−6816.
(6) Sakamoto, K.; Yoshino, S.; Takemoto, M.; Furuya, N. *J. Porphyrins Phthalocyanines* **2013**, *17*, 605−627.
(7) Ding, L. L.; Luan, L. Q.; Shi, J. W.; Liu, W. *Chin. J. Inorg. Chem.* **2013**, *29*, 1591−1598.
(8) Lukyanets, E. A. *J. Porphyrins Phthalocyanines* **1999**, *3*, 424−432.
(9) Garcia-Iglesias, M.; Cid, J. J.; Yum, J. H.; Forneli, A.; Vazquez, P.; Nazeeruddin, M. K.; Palomares, E.; Gratzel, M.; Torres, T. *Energy Environ. Sci.* **2011**, *4*, 189−194.
(10) Hardin, B. E.; Hoke, E. T.; Armstrong, P. B.; Yum, J. H.; Comte, P.; Torres, T.; Frechet, J. M. J.; Nazeeruddin, M. K.; Gratzel, M.; McGehee, M. D. *Nat. Photonics* **2009**, *3*, 667−667.
(11) Li, X. Y.; Wang, H. X.; Wu, H. X. In *Functional Phthalocyanine Molecular Materials*; Jiang, J., Ed.; Structure and Bonding *135*; Springer: Berlin, 2010; pp 229−273.
(12) Lopez-Duarte, I.; Wang, M. K.; Humphry-Baker, R.; Ince, M.; Martinez-Diaz, M. V.; Nazeeruddin, M. K.; Torres, T.; Gratzel, M. *Angew. Chem., Int. Ed.* **2012**, *51*, 1895−1898.
(13) Walter, M. G.; Rudine, A. B.; Wamser, C. C. *J. Porphyrins Phthalocyanines* **2010**, *14*, 759−792.
(14) Ragoussi, M. E.; Ince, M.; Torres, T. *Eur. J. Org. Chem.* **2013**, *2013*, 6475−6489.
(15) Fihri, A.; Artero, V.; Razavet, M.; Baffert, C.; Leibl, W.; Fontecave, M. *Angew. Chem., Int. Ed.* **2008**, *47*, 564−567.
(16) Arachchige, S. M.; Brown, J. R.; Chang, E.; Jain, A.; Zigler, D. F.; Rangan, K.; Brewer, K. J. *Inorg. Chem.* **2009**, *48*, 1989−2000.
(17) Abe, T.; Tobinai, S.; Taira, N.; Chiba, J.; Itoh, T.; Nagai, K. *J. Phys. Chem. C* **2011**, *115*, 7701−7705.
(18) Han, Z. J.; Shen, L. X.; Brennessel, W. W.; Holland, P. L.; Eisenberg, R. *J. Am. Chem. Soc.* **2013**, *135*, 14659−14669.
(19) Natali, M.; Luisa, A.; Iengo, E.; Scandola, F. *Chem. Commun.* **2014**, *50*, 1842−1844.
(20) Stoll, T.; Gennari, M.; Fortage, J.; Castillo, C. E.; Rebarz, M.; Sliwa, M.; Poizat, O.; Odobel, F.; Deronzier, A.; Collomb, M.-N. *Angew. Chem., Int. Ed.* **2014**, *53*, 1654−1658.
(21) Gunaratne, T. C.; Gusev, A. V.; Peng, X. Z.; Rosa, A.; Ricciardi, G.; Baerends, E. J.; Rizzoli, C.; Kenney, M. E.; Rodgers, M. A. J. *J. Phys. Chem. A* **2005**, *109*, 2078−2089.
(22) Kumar, V.; Casella, M.; Molotokaite, E.; Gatti, D.; Kukura, P.; Manzoni, C.; Polli, D.; Marangoni, M.; Cerullo, G. *Phys. Rev. A* **2012**, *86*, No. 053810.
(23) Heiman, D.; Hellwarth, R. W.; Levenson, M. D.; Martin, G. *Phys. Rev. Lett.* **1976**, *36*, 189−192.
(24) Levenson, M. D.; Song, J. J.; Hellwarth, R. W.; Heiman, D. *Opt. Commun.* **1976**, *18*, 133−134.
(25) Levenson, M. D. In *Chemical Applications of Nonlinear Raman Spectroscopy*; Harvey, A. B., Ed.; Academic Press: New York, 1981; pp 205−238.
(26) Shim, S.; Mathies, R. A. *J. Raman Spectrosc.* **2008**, *39*, 1526−1530.

(27) Molotokaite, E.; Kumar, V.; Manzoni, C.; Polli, D.; Cerullo, G.; Marangoni, M. *J. Raman Spectrosc.* **2013**, *44*, 1385−1392.
(28) Bobbitt, D. R.; Yeung, E. S. *Prog. Anal. Spectrosc.* **1986**, *9*, 145−166.
(29) Slipchenko, M. N.; Prince, B. D.; Ducatman, S. C.; Stauffer, H. U. *J. Phys. Chem. A* **2009**, *113*, 135−140.
(30) Bhatia, P. S.; Holder, J. P.; Keto, J. W. *J. Opt. Soc. Am. B* **1997**, *14*, 263−270.
(31) Borysow, J.; Taylor, R. H.; Keto, J. W. *Opt. Commun.* **1988**, *68*, 80−86.
(32) Herrmann, J.; Motschmann, U. *Opt. Quant. Electron.* **1981**, *13*, 19−34.
(33) Garetz, B. A. *Opt. Commun.* **1984**, *49*, 65−66.
(34) Beard, M. C.; Lotshaw, W. T.; Korter, T. M.; Heilweil, E. J.; McMorrow, D. *J. Phys. Chem. A* **2004**, *108*, 9348−9360.
(35) Cong, P.; Deuel, H. P.; Simon, J. D. *Chem. Phys. Lett.* **1995**, *240*, 72−78.
(36) McMorrow, D.; Lotshaw, W. T.; Kenneywallace, G. A. *Chem. Phys. Lett.* **1988**, *145*, 309−314.
(37) Shirota, H. *J. Phys. Chem. B* **2005**, *109*, 7053−7062.
(38) Winkler, K.; Lindner, J.; Bursing, H.; Vohringer, P. *J. Chem. Phys.* **2000**, *113*, 4674−4682.
(39) Deuel, H. P.; Cong, P. J.; Simon, J. D. *J. Raman Spectrosc.* **1995**, *26*, 523−526.
(40) Hyun, B. R.; Quitevis, E. L. *Chem. Phys. Lett.* **2003**, *370*, 725−732.
(41) Lu, R.; Wang, W.; Yuan, S. W.; Yu, A. C. *Chem. Lett.* **2013**, *42*, 63−65.
(42) Shirota, H.; Biswas, R. *J. Phys. Chem. B* **2012**, *116*, 13765−13773.
(43) Shirota, H.; Castner, E. W. *J. Am. Chem. Soc.* **2001**, *123*, 12877−12885.
(44) Giraud, G.; Karolin, J.; Wynne, K. *Biophys. J.* **2003**, *85*, 1903−1913.
(45) Apanasevich, P. A.; Kozich, V. P.; Vodchitz, A. I.; Kontsevoy, B. L. *Inst. Phys. Conf. Ser.* **1992**, 227−230.
(46) Klenerman, D.; Gerrard, D. L.; Herman, H.; Macpherson, M. T. *Chem. Phys. Lett.* **1990**, *168*, 579−583.
(47) Klenerman, D. *Opt. Lett.* **1991**, *16*, 838−839.
(48) Freudiger, C. W.; Roeffaers, M. B. J.; Zhang, X.; Saar, B. G.; Min, W.; Xie, X. S. *J. Phys. Chem. B* **2011**, *115*, 5574−5581.
(49) Rihter, B. D.; Kenney, M. E.; Ford, W. E.; Rodgers, M. A. J. *J. Am. Chem. Soc.* **1990**, *112*, 8064−8070.
(50) Cook, M. J.; Dunn, A. J.; Howe, S. D.; Thomson, A. J.; Harrison, K. J. *J. Chem. Soc., Perkin Trans. 1* **1988**, 2453−2458.
(51) Martinez, O. E. *IEEE J. Quantum Electron.* **1987**, *23*, 59−64.
(52) McCamant, D. W.; Kukura, P.; Yoon, S.; Mathies, R. A. *Rev. Sci. Instrum.* **2004**, *75*, 4971−4980.
(53) Yamaguchi, S.; Hamaguchi, H. O. *Appl. Spectrosc.* **1995**, *49*, 1513−1515.
(54) Kobayashi, N.; Ogata, H.; Nonaka, N.; Luk'yanets, E. A. *Chem.—Eur. J.* **2003**, *9*, 5123−5134.
(55) Lee, J.; Challa, J. R.; McCamant, D. W. *J. Raman Spectrosc.* **2013**, *44*, 1263−1272.
(56) Sun, Z.; Qiu, X. Q.; Lu, J.; Zhang, D. H.; Lee, S. Y. *J. Raman Spectrosc.* **2008**, *39*, 1568−1577.
(57) Umapathy, S.; Mallick, B.; Lakshmanna, A. *J. Chem. Phys.* **2010**, 133.
(58) Kano, H.; Saito, T.; Kobayashi, T. *J. Phys. Chem. A* **2002**, *106*, 3445−3453.
(59) Ma, H. L.; Liu, J.; Liang, W. Z. *J. Chem. Theor. Compt.* **2012**, *8*, 4474−4482.
(60) Spiro, T. G.; Strekas, T. C. *Proc. Natl. Acad. Sci. U.S.A.* **1972**, *69*, 26222626
(61) Sztainbuch, I. W.; Soos, Z. G.; Spiro, T. G. *J. Chem. Phys.* **1994**, *101*, 4644−4648.
(62) Bartholomew, C. R.; McConnell, A. A.; Smith, W. E. *J. Raman Spectrosc.* **1989**, *20*, 595−600.
(63) Huang, T. H.; Chen, W. H.; Rieckhoff, K. E.; Voigt, E. M. *J. Chem. Phys.* **1984**, *80*, 4051−4064.
(64) McConnell, A. A.; Smith, W. E. *J. Raman Spectrosc.* **1989**, *20*, 31−34.
(65) Pawlikowski, M.; Zgierski, M. Z. *Chem. Phys. Lett.* **1980**, *74*, 327−329.
(66) Leng, W.; Kelley, A. M. *J. Phys. Chem. A* **2008**, *112*, 5925−5929.
(67) Bovill, A. J.; McConnell, A. A.; Rospendowski, B. N.; Smith, W. E. *J. Chem. Soc., Faraday Trans.* **1992**, *88*, 455−459.
(68) Braun, D.; Titeca, B. C.; Ceulemans, A. *J. Porphyrins Phthalocyanines* **2001**, *5*, 33−43.
(69) Meyer, K.; Bill, E.; Mienert, B.; Weyhermuller, T.; Wieghardt, K. *J. Am. Chem. Soc.* **1999**, *121*, 4859−4876.
(70) Tobik, J.; Tosatti, E. *J. Phys. Chem. A* **2007**, *111*, 12570−12576.
(71) Liu, Z. Q.; Zhang, X. X.; Zhang, Y. X.; Jiang, J. Z. *Spectrochim. Acta: A—Mol. Biomol. Spectrosc.* **2007**, *67*, 1232−1246.
(72) Sumimoto, M.; Kawashima, Y.; Hori, K.; Fujimoto, H. *Spectrochim. Acta: A—Mol. Biomol. Spectrosc.* **2008**, *71*, 286−287.
(73) Zhang, X. X.; Bao, M.; Pan, N.; Zhang, Y. X.; Jiang, J. Z. *Chin. J. Chem.* **2004**, *22*, 325−332.
(74) Zhang, X. X.; Zhang, Y. X.; Jiang, J. Z. *Vib. Spectrosc.* **2003**, *33*, 153−161.
(75) Li, D. C.; Peng, Z. H.; Deng, L. Z.; Shen, W. F.; Zhou, Y. H. *Vib. Spectrosc.* **2005**, *39*, 191−199.
(76) Liu, Z. Q.; Chen, Z. X.; Jin, B. B.; Zhang, X. X. *Vib. Spectrosc.* **2011**, *56*, 210−218.
(77) Saini, G. S. S.; Dogra, S. D.; Sharma, K.; Singh, S.; Tripathi, S. K.; Sathe, V.; Singh, R. K. *Vib. Spectrosc.* **2011**, *57*, 61−71.
(78) Pouladsaz, D.; Schreiber, M.; Gopakumar, T. G. *J. Chem. Phys.* **2013**, 138.
(79) Tackley, D. R.; Dent, G.; Smith, W. E. *Phys. Chem. Chem. Phys.* **2000**, *2*, 3949−3955.
(80) Bovill, A. J.; McConnell, A. A.; Nimmo, J. A.; Smith, W. E. *J. Phys. Chem.* **1986**, *90*, 569−575.
(81) Basova, T. V.; Kiselev, V. G.; Schuster, B. E.; Peisert, H.; Chasse, T. *J. Raman Spectrosc.* **2009**, *40*, 2080−2087.
(82) Soldatova, A. V.; Kim, J.; Peng, X. H.; Rosa, A.; Ricciardi, G.; Kenney, M. E.; Rodgers, M. A. J. *Inorg. Chem.* **2007**, *46*, 2080−2093.
(83) Abraham, J. P.; Sajan, D.; Shettigar, V.; Dharmaprakash, S. M.; Nemec, I.; Joe, I. H.; Jayakumar, V. S. *J. Mol. Struct.* **2009**, *917*, 27−36.
(84) Castaneda, I. C. H.; Jios, J. L.; Piro, O. E.; Tobon, G. E.; Della Vedova, C. O. *J. Mol. Struct.* **2007**, *842*, 46−54.
(85) Takeuchi, H.; Watanabe, N.; Harada, I. *Spectrochim. Acta: A—Mol. Spectrosc.* **1988**, *44*, 749−761.
(86) Howe, L.; Zhang, J. Z. *J. Phys. Chem. A* **1997**, *101*, 3207−3213.
(87) Anusha, P. T.; Swain, D.; Hamad, S.; Giribabu, L.; Prashant, T. S.; Tewari, S. P.; Rao, S. V. *J. Phys. Chem. C* **2012**, *116*, 17828−17837.
(88) Kaneko, Y.; Arai, T.; Sakuragi, H.; Tokumaru, K.; Pac, C. *J. Photochem. Photobiol., A* **1996**, *97*, 155−162.
(89) Parthasarathi, N.; Hansen, C.; Yamaguchi, S.; Spiro, T. G. *J. Am. Chem. Soc.* **1987**, *109*, 3865−3871.